High-Resolution Surface-Wave Tomography from Ambient Seismic Noise

Nikolai M. Shapiro, *et al.*

Science **307**, 1615 (2005);
DOI: 10.1126/science.1108339

Science (print ISSN 0036-8075; online ISSN 1095-9203) is published weekly, except the last week in December, by the American Association for the Advancement of Science, 1200 New York Avenue NW, Washington, DC 20005.

References and Notes

1. W. J. Bartz, Ed., *Engines and Automotive Lubrication* (Marcel Dekker, New York, 1993).
2. I. M. Hutchings, Ed., *Friction, Lubrication and Wear of Artificial Joints* (Professional Engineering Publishing, Bury St. Edmunds, UK, 2003).
3. B. Bhushan, *Tribology and Mechanics of Magnetic Storage Devices* (Springer-Verlag, New York, ed. 2, 1996).
4. H. P. Jost, *Wear* **136**, 1 (1990).
5. M. Urbakh, J. Klafter, D. Gourdon, J. Israelachvili, *Nature* **430**, 525 (2004).
6. U. Raviv, J. Klein, *Science* **297**, 1540 (2002).
7. B. Bhushan, J. B. Israelachvili, U. Landman, *Nature* **374**, 607 (1995).
8. S. Granick, *Phys. Today* **52**, 26 (1999).
9. M. Cieplak, E. D. Smith, M. O. Robbins, *Science* **265**, 1209 (1994).
10. M. Abdelmaksoud, J. W. Bender, J. Krim, *Phys. Rev. Lett.* **92**, 176101 (2004).
11. Z. Pawlak, *Tribochemistry of Lubricating Oils* (Elsevier, Amsterdam, 2003).
12. This has led to stricter controls on the concentrations of these elements in engine oils, which has limited the amount of ZDDP that can be incorporated into motor oil formulations.
13. The replacement of steel by aluminum is motivated by efforts to reduce vehicle weight as a means of improving fuel efficiency. For example, it has been estimated that a 10% reduction in vehicle weight can result in a 7% improvement in fuel economy. However, because of the inability of ZDDPs to adequately protect aluminum surfaces, automobile manufacturers have had to resort to engines composed of aluminum-based composite materials or to engine blocks that contain steel sleeves. These measures are costly and complicate engine fabrication.
14. M. L. Suominen Fuller, M. Kasrai, G. M. Bancroft, K. Fyfe, K. H. Tan, *Tribol. Int.* **31**, 627 (1999).
15. J. M. Martin, C. Grossiord, T. Le Mogne, S. Bec, A. Tonck, *Tribol. Int.* **34**, 523 (2001).
16. P. A. Willermet, D. P. Dailey, R. O. Carter III, P. J. Schmitz, W. Zhu, *Tribol. Int.* **28**, 177 (1995).
17. Y. Wan *et al.*, *Tribol. Ser.* **40**, 155 (2002).
18. Experiments show that zinc phosphate films almost 100 nm high can be formed after a few minutes of rubbing (*44*). The real contact time at the molecular level is significantly less than the rubbing time, because only a small fraction of the asperities are in contact with the opposing surface at a given time.
19. M. A. Nicholls *et al.*, *Tribol. Lett.* **17**, 205 (2004).
20. H. Spikes, *Tribol. Lett.* **17**, 469 (2004).
21. M. A. Nicholls, T. Do, P. R. Norton, M. Kasrai, G. M. Bancroft, *Tribol. Int.* **38**, 15 (2005).
22. A. B. Tutein, S. J. Stuart, J. A. Harrison, *Langmuir* **16**, 291 (2000).
23. G. He, M. H. Müser, M. O. Robbins, *Science* **284**, 1650 (1999).
24. J. A. Harrison, D. W. Brenner, *J. Am. Chem. Soc.* **116**, 10399 (1994).
25. S. Bair, C. McCabe, P. T. Cummings, *Phys. Rev. Lett.* **88**, 058302 (2002).
26. S. Jiang *et al.*, *J. Phys. Chem.* **100**, 15760 (1996).
27. N. J. Mosey, T. K. Woo, *J. Phys. Chem. A* **107**, 5058 (2003).
28. M. A. Wimmer, C. Sprecher, R. Hauert, G. Täger, A. Fischer, *Wear* **255**, 1007 (2003).
29. U. Landman, W. D. Luedtke, J. P. Gao, *Langmuir* **12**, 4514 (1996).
30. R. Car, M. Parinello, *Phys. Rev. Lett.* **55**, 2471 (1985).
31. M. Parrinello, *Solid State Commun.* **38**, 115 (1997).
32. C. Cavazzoni *et al.*, *Science* **283**, 44 (1999).
33. D. Alfè, M. J. Gillan, G. D. Price, *Nature* **401**, 462 (1999).
34. All AIMD simulations were performed with the CPMD software package (*45*). The potential energy was calculated using Kohn-Sham density functional theory with the gradient-corrected exchange-correlation functional of Perdew, Burke, and Ernzerhof (*46*); Troullier-Martins–type pseudopotentials; and a Γ-point plane wave expansion of the valence orbitals up to 120 Ry. A time step of 2.0 atomic units, equivalent to 0.0483 fs, was used in all simulations. Pressure was applied isotropically using the Parrinello-Rahman variable cell method (*47*, *48*), and preliminary calculations showed that well-converged values for the pressure were achieved using the theoretical approach outlined above. Temperatures of 100 and 1000 K were considered, with most simulations being performed at 100 K to isolate the effect of pressure. To give the reader an idea of the computational effort associated with these simulations, it is noted that one complete c/d cycle over a range of 0.25 to 32.5 GPa at 2.5 GPa/ps required nearly 5 weeks of CPU time on a Beowulf cluster of 24 Compaq Alpha ES40 computers running at 833 MHz.
35. A four-coordinate see-saw geometry can be derived by removing any two adjacent bond sites from a central atom with an originally six-coordinate octahedral geometry.
36. M. H. Müser, *Phys. Rev. Lett.* **89**, 224301 (2002).
37. The logarithmic-type dependence of the underlying chemical reactions on the compression rate can be rationalized within Eyring theory.
38. B. N. J. Persson, *J. Chem. Phys.* **115**, 3840 (2001).
39. S. Bec *et al.*, *Proc. R. Soc. London Ser. A* **455**, 4181 (1999).
40. J. F. Graham, C. McCague, P. R. Norton, *Tribol. Lett.* **6**, 149 (1999).
41. J. S. Sheasby, T. A. Caughlin, W. A. Mackwood, *Wear* **201**, 209 (1996).
42. M. Fuller *et al.*, *Tribol. Lett.* **1**, 367 (1995).
43. Z. Wisniewski, R. Wisniewski, J. L. Nowinski, *Solid State Ionics* **157**, 275 (2003).
44. M. Aktary, M. T. McDermott, G. A. McApline, *Tribol. Lett.* **12**, 155 (2002).
45. J. Hütter *et al.*, *CPMD* (MPI für Festkörperforschung Stuttgart and IBM Zurich Research Laboratory, Rueschlikon, Switzerland, 1995-2001).
46. J. P. Perdew, K. Burke, M. Ernzerhof, *Phys. Rev. Lett.* **77**, 3865 (1996).
47. M. Parrinello, A. Rahman, *Phys. Rev. Lett.* **45**, 1196 (1980).
48. P. Focher, G. L. Chiarotti, M. Bernasconi, E. Tosatti, M. Parrinello, *Europhys. Lett.* **36**, 345 (1994).

49. We thank P. R. Norton for inspiring us to work on this topic and P. R. Norton, M. Kasrai, Y.-T. Cheng, and W. Capehart for many useful discussions. The Natural Science and Engineering Research Council of Canada and General Motors R&D are acknowledged for providing financial support. Computational resources were made available by the Canadian Foundation for Innovation and SHARCNet of Canada.

24 November 2004; accepted 25 January 2005
10.1126/science.1107895

High-Resolution Surface-Wave Tomography from Ambient Seismic Noise

Nikolai M. Shapiro,[1]* Michel Campillo,[2] Laurent Stehly,[2] Michael H. Ritzwoller[1]

Cross-correlation of 1 month of ambient seismic noise recorded at USArray stations in California yields hundreds of short-period surface-wave group-speed measurements on interstation paths. We used these measurements to construct tomographic images of the principal geological units of California, with low-speed anomalies corresponding to the main sedimentary basins and high-speed anomalies corresponding to the igneous cores of the major mountain ranges. This method can improve the resolution and fidelity of crustal images obtained from surface-wave analyses.

The aim of ambitious new deployments of seismic arrays, such as the Program for the Array Seismic Studies of the Continental Lithosphere (PASSCAL) and USArray programs (*1*), is to improve the resolution of images of Earth's interior by adding more instruments to regional- and continental-scale seismic networks. Traditional observational methods cannot fully exploit emerging array data because they are based on seismic waves emitted from earthquakes, which emanate from select source regions predominantly near plate boundaries and are observed at stations far from the source regions, such as most locations within the United States. With such teleseismic observations, high-frequency information is lost because of intrinsic attenuation and scattering, and resolution is degraded by the spatial extent of the surface wave's sensitivity, which expands with path length (*2*–*4*). We have moved beyond the limitations of methods based on earthquakes and recovered surface-wave dispersion data from ambient seismic noise (*5*).

The basic idea of the new method is that cross-correlation of a random isotropic wavefield computed between a pair of receivers will result in a waveform that differs only by an amplitude factor from the Green function between the receivers (*6*, *7*). This property is reminiscent of the fluctuation-dissipation theorem (*8*), which posits a relation between the random fluctuations of a linear system and the system's response to an external force. The relation is widely used in a variety of physical applications and has its roots in early works on Brownian noise (*9*, *10*). Recent results in helioseismology (*11*), acoustics (*12*–*16*), and seismology (*5*, *17*)

[1]Center for Imaging the Earth's Interior, Department of Physics, University of Colorado at Boulder, Boulder, CO, USA. [2]Laboratoire de Géophysique Interne et de Tectonophysique, Université Joseph Fourier, Grenoble, France.

*To whom correspondence should be addressed. E-mail: nshapiro@ciei.colorado.edu

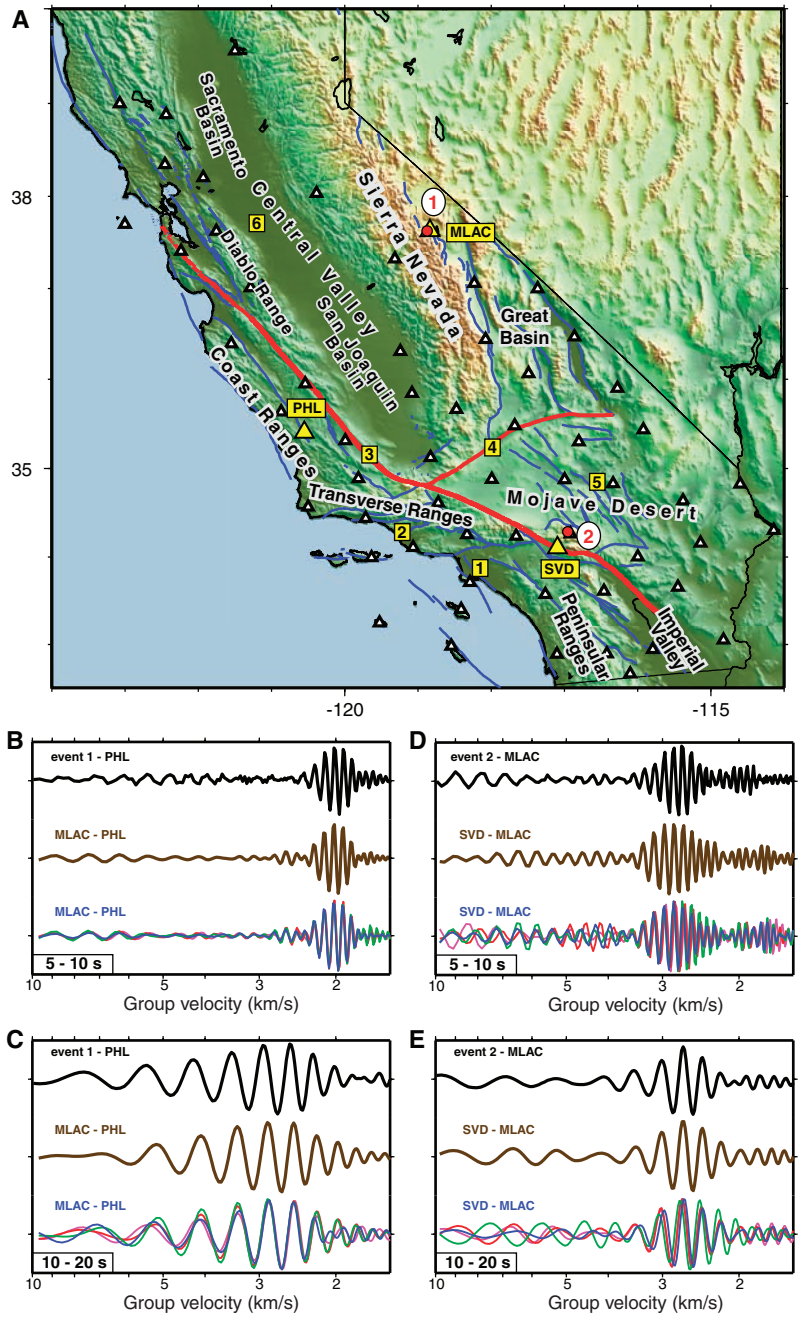

Fig. 1. Waveforms emerging from cross-correlations of ambient seismic noise compared with Rayleigh waves excited by earthquakes. (**A**) Reference map showing the locations of the principal geographical and geological features discussed in the text. White triangles show the locations of the USArray stations used in this study (5 of the 62 stations are located north of 40°N). Blue and red solid lines are the locations of known active faults. Yellow rectangles with digits indicate the following features: (1) Los Angeles Basin, (2) Ventura Basin, (3) San Andreas Fault, (4) Garlock Fault, (5) Mojave shear zone, and (6) Stockton Arch. (**B**) Comparison of waves propagating between stations MLAC and PHL [yellow triangles in (A)], bandpassed over periods between 5 and 10 s. The upper trace (black) is the signal emitted by earthquake 1 [white circle with red number in (A)] near MLAC observed at PHL; the middle trace (gold) is the cross-correlation from 1 year of ambient seismic noise observed at stations MLAC and PHL; and the lower traces are cross-correlations from 4 separate months of noise observed at the two stations in 2002 (magenta, January; red, April; green, July; blue, October). The earthquake-emitted signal was normalized to the spectrum of the cross-correlated ambient noise. (**C**) Similar to (B), but with the bandpass filter at periods between 10 and 20 s. (**D**) Similar to (B), but between stations SVD and MLAC [yellow triangles in (A)]. Earthquake 2 is near station SVD, observed at station MLAC. (**E**) Similar to (D), but with the bandpass filter at periods between 10 and 20 s.

suggest that such a statistical treatment can be applied to nonthermal random wavefields, in particular to long series of ambient seismic noise, because the distribution of the ambient sources randomizes when averaged over long times. Ambient seismic noise is additionally randomized by scattering from heterogeneities within Earth (*18*). Surface waves are most easily extracted from the ambient noise (*5*), because they dominate the Green function between receivers located at the surface and also because ambient seismic noise is excited preferentially by superficial sources, such as oceanic microseisms and atmospheric disturbances (*19*–*22*). The seismic noise field is often not perfectly isotropic and may be dominated by waves arriving from a few principal directions. To reduce the contribution of the most energetic arrivals, we disregard the amplitude by correlating only one-bit signals (*15*, *17*) before the computation of the cross-correlation.

Examples of cross-correlations between pairs of seismic stations in California appear in Fig. 1 (*23*). Cross-correlations between two station pairs (MLAC-PHL and SVD-MLAC) in two short-period bands (5 to 10 s and 10 to 20 s) are presented using four different 1-month time series (January, April, July, and October 2002). For each station pair, results from different months are similar to one another and to the results produced by analyzing a whole year of data, but differ between the station pairs. Thus, the emerging waveforms are stable over time and characterize the structure of the earth between the stations. In addition, the cross-correlations of noise sequences are very similar to surface waves emitted by earthquakes near one receiver observed at the other receiver. This confirms that the cross-correlations approximate Green functions of Rayleigh waves propagating between each pair of stations and that 1 month of data suffices to extract Rayleigh-wave Green functions robustly in the period band of interest here (7 to 20 s).

We selected 30 relatively quiescent days (during which no earthquakes stronger than magnitude 5.8 occurred) of continuous data taken at a rate of one sample per second from 62 USArray stations within California (*24*) during August and September 2004. Short-period surface-wave dispersion curves are estimated from the Green functions using frequency-time analysis (*25*–*27*) from the 1891 paths connecting these stations. We rejected waveforms with signal-to-noise ratios smaller than 4 and for paths shorter than two wavelengths, resulting in 678 and 891 group-speed measurements at periods of 7.5 and 15 s, respectively (fig. S2). We then applied a tomographic inversion (*28*) to these two data sets to obtain group-speed maps on a 28 × 28 km grid across California (Fig. 2).

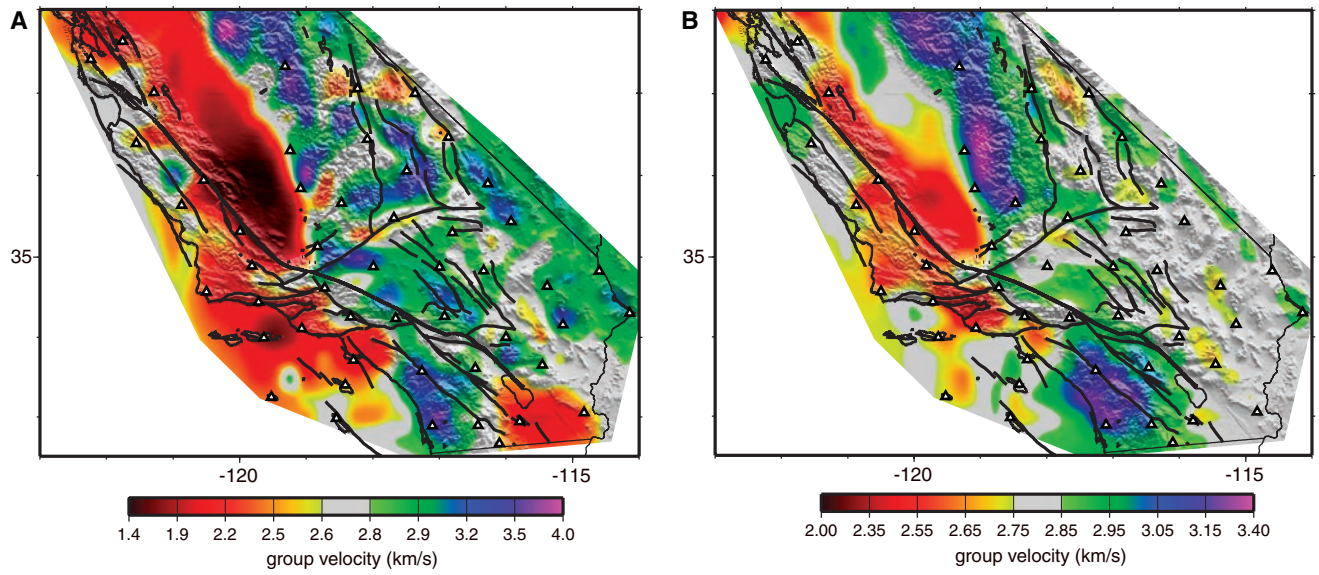

Fig. 2. Group-speed maps constructed by cross-correlating 30 days of ambient noise between USArray stations. (**A**) 7.5-s-period Rayleigh waves. (**B**) 15-s-period Rayleigh waves. Black solid lines show known active faults. White triangles show locations of USArray stations used in this study. Similar maps from a different single month of data are shown in the supporting online material.

The maps produced variance reductions of 93 and 76% at 7.5 and 15 s, respectively, relative to the regional average speed at each period. To test the robustness of the inversion, we applied the same procedure to a second month of data and produced similar tomographic maps (fig. S3). The resolution of the resulting images is about the average interstation distance, between 60 and 100 km across most of each map (fig. S4).

A variety of geological features (*29*) are recognizable in the estimated group-speed dispersion maps (Fig. 2). For the 7.5-s Rayleigh wave, which is most sensitive to shallow crustal structures no deeper than about 10 km, the dispersion map displays low group speeds for the principal sedimentary basins in California, including the basins in the Central Valley, the Salton Trough in the Imperial Valley, the Los Angeles Basin, and the Ventura Basin. Regions consisting mainly of plutonic rocks (the Sierra Nevada, the Peninsular Ranges, the Great Basin, and the Mojave Desert region) are characterized predominantly by fast group speeds. Somewhat lower speeds are observed in the Mojave Shear Zone and along the Garlock Fault. The Coast Ranges, the Transverse Ranges, and the Diablo Range, which are mainly composed of sedimentary rocks, are characterized by low group speeds, with the exception of the Salinian block located south of Monterey Bay.

For the 15-s Rayleigh wave, which is sensitive mainly to the middle crust down to depths of about 20 km, very fast group speeds correspond to the remnants of the Mesozoic volcanic arc: the Sierra Nevada and the Peninsular Ranges, composed principally of Cretaceous granitic batholiths. The map also reveals the contrast between the western and eastern parts of the Sierra Nevada (*30*). The group speeds are lower in the Great Basin and in the Mojave Desert, indicating that the middle crust in these areas is probably hotter and weaker than in the Sierra Nevada. In the Central Valley, slow group speeds are associated with two deep sedimentary basins: the San Joaquin Basin in the south and the Sacramento Basin in the north, separated in the middle by the igneous-dominated Stockton Arch (*31*). Group speeds are low in the sedimentary mountain ranges (the Transverse Ranges, the southern part of the Coast Ranges, and the Diablo Range). Neutral to fast wave speeds are observed for the Salinian block. In this area, the 15-s map shows a contrast between the high-speed western wall of the San Andreas Fault, composed of plutonic rocks of the Salinian block, and its low-speed eastern wall, composed of sedimentary rocks of the Franciscan formation.

These results establish that Rayleigh-wave Green functions extracted by cross-correlating long sequences of ambient seismic noise, which are discarded as part of traditional seismic data processing, contain information about the structure of the shallow and middle crust. The use of ambient seismic noise as the source of seismic observations addresses several shortcomings of traditional surface-wave methods. The method is particularly advantageous in the context of temporary seismic arrays such as the Transportable Array component of USArray or PASSCAL experiments, because it can return useful information even if earthquakes do not occur. The short-period dispersion maps produced by the method can provide homogeneously distributed information about shear wave speeds in the crust, which are hard to acquire with traditional methods. The new method enhances resolution because measurements are made between regularly spaced receivers, which may lie much closer to one another than to earthquakes.

It may seem initially surprising that deterministic information about Earth's crust can result from correlations of ambient seismic noise. This result reminds us that random fluctuations can, in fact, yield the same information as that provided by probing a system with an external force (*9*) and that not all noise is bad. In seismology, external probing through active seismic sources (such as explosions) may be prohibitively expensive, and earthquakes are both infrequent and inhomogeneously distributed. In many instances, merely "listening" to ambient noise may be a more reliable and economical alternative.

References and Notes

1. USArray (www.iris.iris.edu/USArray) is one of the components of the new EarthScope (www.earthscope.org) initiative in the United States. PASSCAL (www.iris.edu/about/PASSCAL) is a program of the Incorporated Research Institutions for Seismology (IRIS) (www.iris.edu).
2. G. Nolet, F. A. Dahlen, *J. Geophys. Res.* **105**, 19043 (2000).
3. J. Spetzler, J. Trampert, R. Snieder, *Geophys. J. Int.* **149**, 755 (2002).
4. M. H. Ritzwoller, N. M. Shapiro, M. P. Barmin, A. L. Levshin, *J. Geophys. Res.* **107**, 2235 (2002).
5. N. M. Shapiro, M. Campillo, *Geophys. Res. Lett.* **31**, L07614, 10.1029/2004GL019491 (2004).
6. R. L. Weaver, O. I. Lobkis, *Phys. Rev. Lett.* **87**, paper 134301 (2001).
7. R. Snieder, *Phys. Rev. E* **69**, 046610 (2004).
8. R. Kubo, *Rep. Prog. Phys.* **29**, 255 (1966).
9. S. Kos, P. Littlewood, *Nature* **431**, 29 (2004).
10. A. Einstein, *Ann. Phys.* **17**, 549 (1905).

11. T. L. Duvall, S. M. Jefferies, J. W. Harvey, M. A. Pomerantz, *Nature* **362**, 430 (1993).
12. R. L. Weaver, O. I. Lobkis, *J. Acoust. Soc. Am.* **110**, 3011 (2001).
13. A. Derode *et al.*, *J. Acoust. Soc. Am.* **113**, 2973 (2003).
14. P. Roux, W. A. Kuperman, *J. Acoust. Soc. Am.* **116**, 1995 (2004).
15. E. Larose, A. Derode, M. Campillo, M. Fink, *J. Appl. Phys.* **95**, 8393 (2004).
16. A. E. Malcolm, J. A. Scales, B. A. van Tiggelen, *Phys. Rev. E* **70**, 10.1103/PhysRevE.70.015601 (2004).
17. M. Campillo, A. Paul, *Science* **299**, 547 (2003).
18. R. Hennino *et al.*, *Phys. Rev. Lett.* **86**, 3447 (2001).
19. A. Friedrich, F. Kruger, K. Klinge, *J. Seismol.* **2**, 47 (1998).
20. T. Tanimoto, *Geophys. J. Int.* **136**, 395 (1999).
21. G. Ekström, *J. Geophys. Res.* **106**, 26483 (2001).
22. J. Rhie, B. Romanowicz, *Nature* **431**, 552 (2004).
23. Data processing was performed with the Seismic Analysis Code (SAC) (*32*).
24. We used 62 stations of the Transportable Array component of USArray in California (Fig. 1A). This includes 40 permanent stations of the Southern California TriNet system (www.trinet.org), 17 permanent stations of the Berkeley Digital Seismic Network (quake.geo.berkeley.edu/bdsn), 2 permanent stations of the Anza Seismic Network (eqinfo.ucsd.edu/deployments/anza.html), and 3 new USArray stations.
25. A. L. Levshin *et al.*, *Seismic Surface Waves in a Laterally Inhomogeneous Earth*, V. I. Keilis-Borok, Ed. (Kluwer Academic, Norwell, MA, 1989).
26. M. H. Ritzwoller, A. L. Levshin, *J. Geophys. Res.* **103**, 4839 (1998).
27. N. M. Shapiro, S. K. Singh, *Bull. Seism. Soc. Am.* **89**, 1138 (1999).
28. M. P. Barmin, M. H. Ritzwoller, A. L. Levshin, *Pure Appl. Geophys.* **158**, 1351 (2001).
29. C. W. Jennings, geologic map of California (California Division of Mines and Geology, Map No. 2, 1977).
30. C. H. Jones, H. Kanamori, S. W. Roecker, *J. Geophys. Res.* **99**, 4567 (1994).
31. A. M. Wilson, G. Garven, J. R. Boles, *GSA Bull.* **111**, 432 (1999).
32. P. Goldstein, L. Minner, *Seism. Res. Lett.* **67**, 39 (1996) (www.llnl.gov/sac).
33. The data used in this work were obtained from the IRIS Data Management Center. We are also particularly grateful to M. Barmin for help with the tomographic code and P. Goldstein for clarifications about the SAC program. We thank C. Jones for a tutorial on the geology of California and E. Larose, O. Lobkis, L. Margerin, R. Maynard, A. Paul, B. van Tiggelen, and R. Weaver for helpful discussions. We acknowledge the support from CNRS/Institut National des Sciences de l'Univers (program DyETI) and the Commissariat à l'Energie Atomique (France).

Supporting Online Material
www.sciencemag.org/cgi/content/full/307/5715/1615/DC1
Figs. S1 to S4

6 December 2004; accepted 19 January 2005
10.1126/science.1108339

Worldwide Phylogeography of Wild Boar Reveals Multiple Centers of Pig Domestication

Greger Larson,[1]* Keith Dobney,[2] Umberto Albarella,[3] Meiying Fang,[4] Elizabeth Matisoo-Smith,[5] Judith Robins,[5] Stewart Lowden,[6] Heather Finlayson,[7] Tina Brand,[8] Eske Willerslev,[1] Peter Rowley-Conwy,[2] Leif Andersson,[4] Alan Cooper[1]*†

Mitochondrial DNA (mtDNA) sequences from 686 wild and domestic pig specimens place the origin of wild boar in island Southeast Asia (ISEA), where they dispersed across Eurasia. Previous morphological and genetic evidence suggested pig domestication took place in a limited number of locations (principally the Near East and Far East). In contrast, new genetic data reveal multiple centers of domestication across Eurasia and that European, rather than Near Eastern, wild boar are the principal source of modern European domestic pigs.

The domestication of plants and animals led to one of the most important socioeconomic transitions in human history, yet little is known about whether the process took place in a limited number of geographic regions or was a more widespread innovation involving multiple, independent "events." Wild boar were important prey animals for early hunter-gatherers across wide areas of Eurasia (*1*) until the early Holocene, when this predator-prey relation radically shifted as they, and several other large mammals, were domesticated. An extensive zooarcheological record suggests that pigs were first domesticated ~9000 years ago in the Near East (*2*), whereas more recent molecular and archaeological evidence suggests a second, independent domestication in the Far East (*3*, *4*). In eastern Anatolia, several sites record gradual changes in pig morphology and demographic profile (principally a reduction in certain tooth dimensions and the increased predominance of younger animals in archaeological assemblages) (*5*, *6*) over several millennia, and these have been taken to represent the domestication process in situ. Although the independent domestication of wild boar in Europe has been suggested (*7*), others have concluded that, like cattle (*8*) and sheep, pigs derived from Near Eastern genetic stock were imported by Neolithic farmers into Europe (*9*).

The wild progenitors of many Eurasian domesticates are either extinct [e.g., the aurochs (*8*) and the wild horse (*10*)] or have little or no phylogeographic structure [e.g., the wolf (*11*)]. Consequently, the broad distribution of surviving wild boar populations across the Old World provides a unique opportunity to analyze the origins of modern domestic lineages. Previous studies (*3*, *12*) have identified three divergent clusters of *Sus scrofa* mitochondrial sequences, one Asian clade and two European groups, of which one consists solely of Italian wild boar. Both the Asian and European groups contain domestic breeds, yet molecular clock estimates indicate the split between the two groups significantly predates evidence for pig domestication, which suggests independent domestication events in each area from divergent wild boar lineages (*3*, *12*).

To investigate the relationships between domestic pigs and indigenous wild boar across their range, we sequenced 663 base pairs (bp) of the mitochondrial control region from 165 wild and feral pigs primarily from museum specimens, using appropriate ancient-DNA methods (*13*), and from 58 domestic pigs. An additional 463 individual pig sequences were obtained from GenBank, and phylogenetic analyses were performed using Bayesian Monte Carlo–Markov chain (MCMC) (*14*) and median-joining networks (*15*). The consensus tree (Fig. 1) shows that the basal lineages of *S. scrofa* occur in western island Southeast Asia (ISEA). An initial dispersal from this area into the Indian subcontinent was followed by subsequent radiations into East Asia and a final, progressive spread across Eurasia into Western Europe. The marked East-West split among wild boar is consistent with morpho-

[1]Henry Wellcome Ancient Biomolecules Centre, University of Oxford, Department of Zoology, South Parks Road OX1 3PS, UK. [2]Department of Archaeology, University of Durham, South Road, Durham DH1 3L, UK. [3]Department of Archaeology, University of Sheffield, West Street, Sheffield S1 4ET, UK. [4]Department of Animal Breeding and Genetics, Swedish University of Agricultural Sciences and Department of Medical Biochemistry and Microbiology, Uppsala University, Uppsala Biomedical Center, Box 597, SE-75124 Uppsala, Sweden. [5]Department of Anthropology and Allan Wilson Centre for Molecular Ecology and Evolution, University of Auckland, P.B. 92019, Auckland, New Zealand. [6]Jurox Pty Limited, 85 Gardiners Road, Rutherford, NSW, 2320, Australia. [7]Department of Genomics and Bioinformatics, Roslin Institute, Roslin, Midlothian, EH25 9PS, UK. [8]Department of Evolutionary Biology, Zoological Institute, University of Copenhagen, Universitetsparken 15, DK-2100, Copenhagen O, Denmark.

*To whom correspondence should be addressed. E-mail: greger.larson@zoo.ox.ac.uk (G.L.) and alan.cooper@adelaide.edu.au (A.C.)
†Present address: School of Environmental Sciences, University of Adelaide, Adelaide, SA 5005, Australia.

Supporting Online Material

High resolution surface wave tomography from ambient seismic noise

Nikolai M. Shapiro[1], Michel Campillo[2], Laurent Stehly[2], Michael H. Ritzwoller[1]

[1]Center for Imaging the Earth's Interior, Department of Physics,
University of Colorado at Boulder, USA
[2]Laboratoire de Géophysique Interne et de Tectonophysique,
Université Joseph Fourier, Grenoble, France

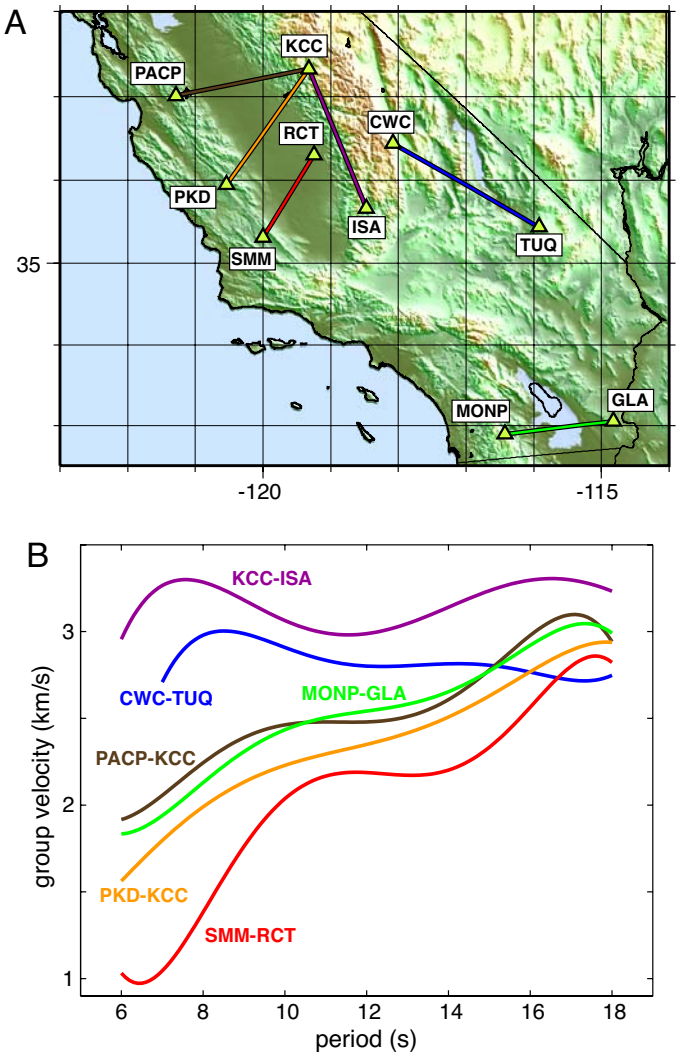

Fig. S1. Group speed curves measured in various parts of California by cross-correlating 30 days of ambient noise between USArray stations. (A) Map showing the station locations and inter-station paths. (B) Group speed dispersion curves between periods of 6 s and 18 s.

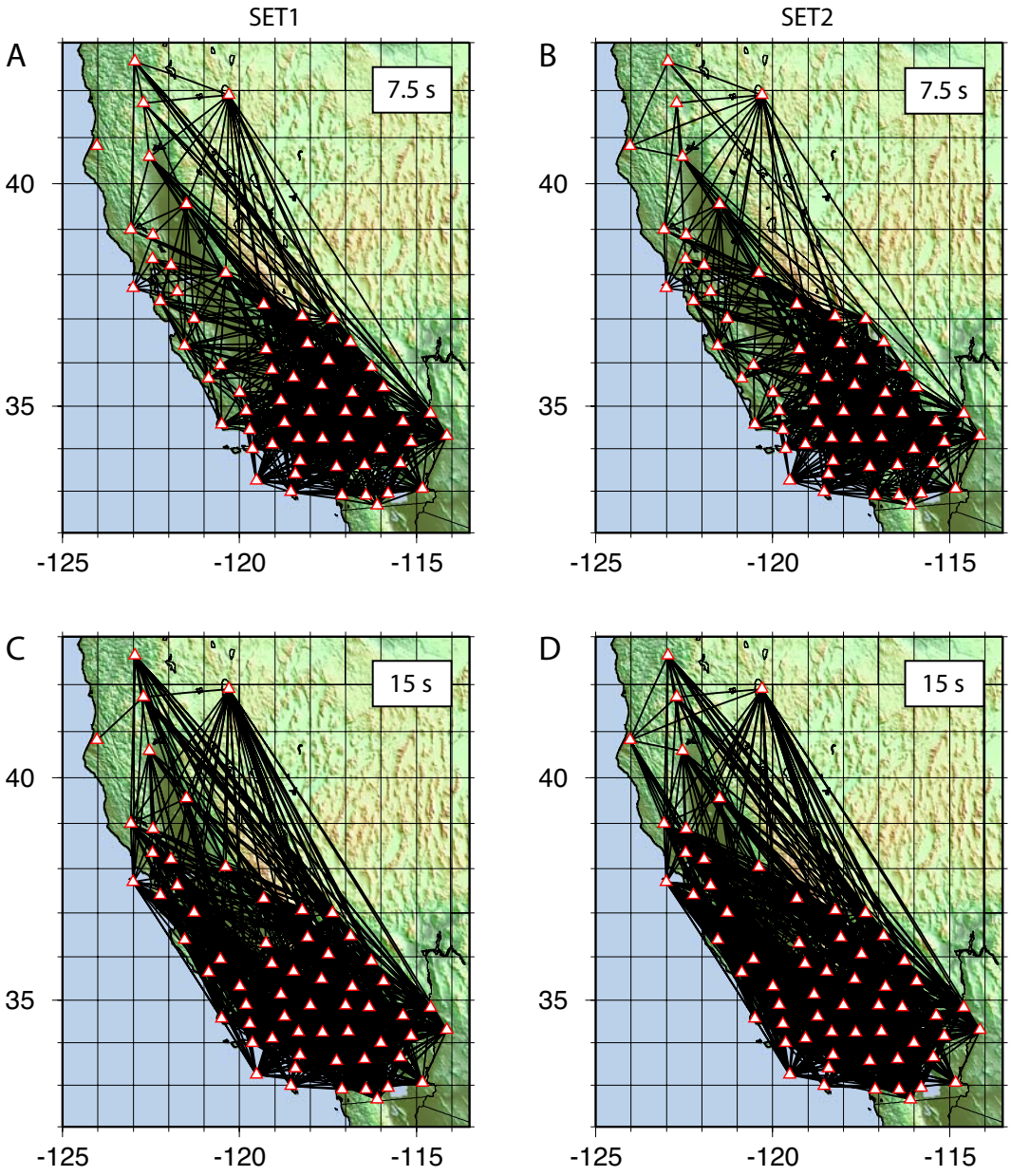

Fig. S2. Paths where Rayleigh wave group speed measurements were obtained from cross-correlations of ambient seismic noise. Cross-correlations were computed from two different 30-day periods. The first of these periods (SET1) was used to construct the Rayleigh wave group speed tomographic maps shown in Fig. 2 of the text. (A) and (B) 7.5 s period Rayleigh wave maps from SET1 and SET2. (C) and (D) 15 s period Rayleigh wave maps from SET1 and SET2. White triangles show locations of USArray stations used in this study.

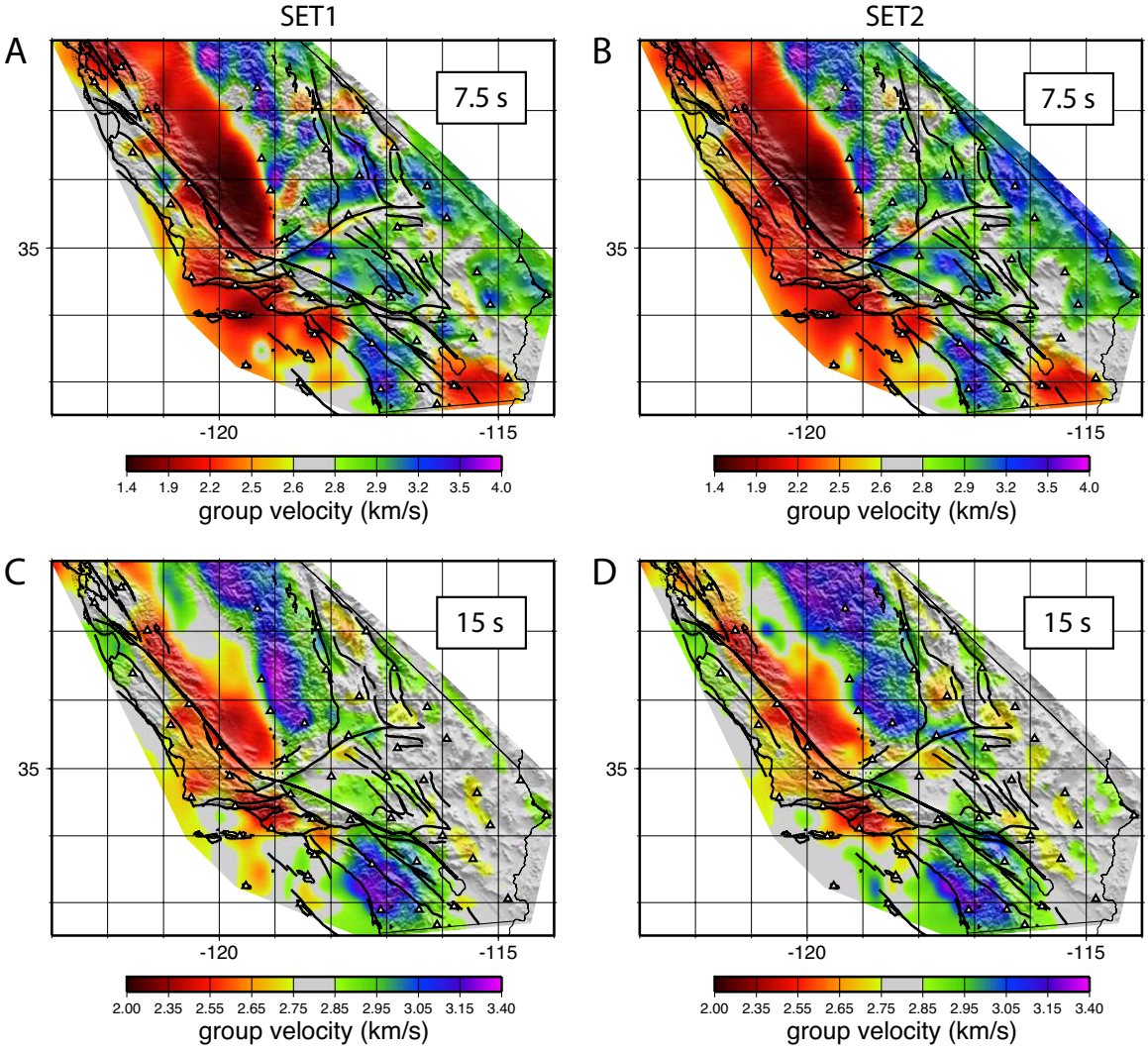

Fig. S3. Group speed maps constructed by cross-correlating two different 30-day periods of ambient noise between USArray stations. (A) and (B) 7.5 s period Rayleigh waves. (C) and (D) 15 s period Rayleigh waves. (A) and (C) Results obtained with SET1, the first data set (shown in the text). (B) and (D) Results obtained with the SET2, the second data set. Black solid lines are active faults. White triangles are locations of USArray stations used in this study.

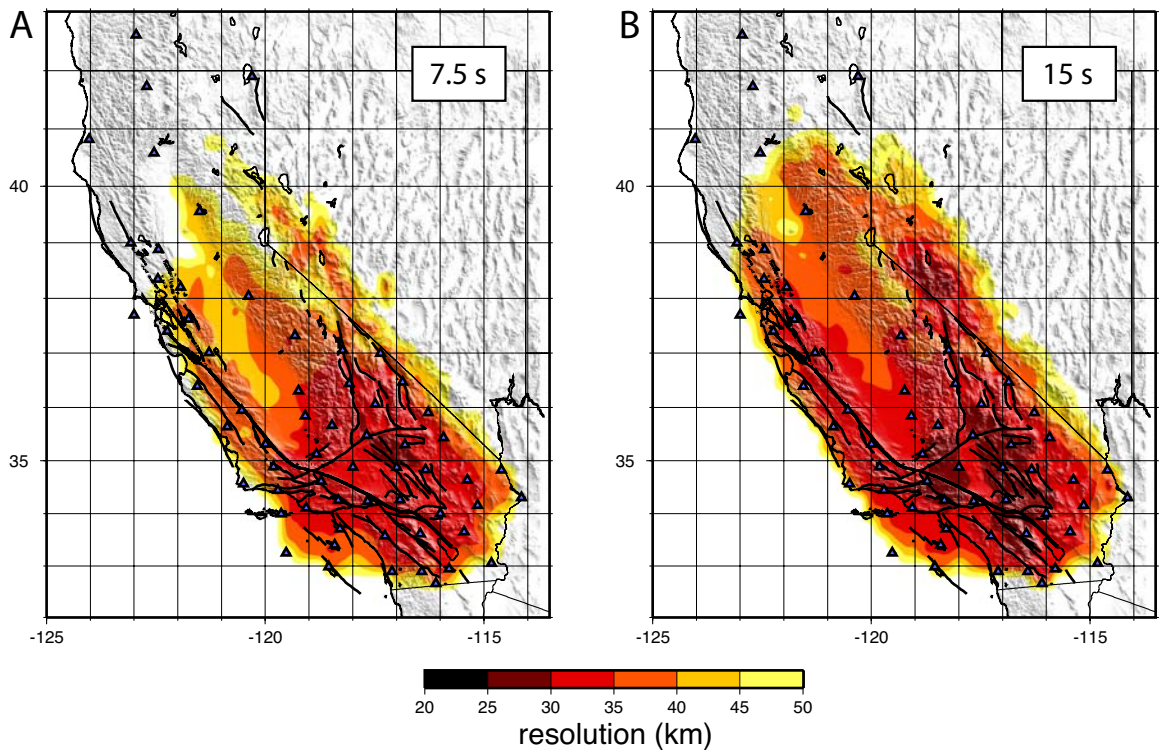

Fig. S4. Resolution of group speed maps obtained with the first data set, SET1 (shown in the text). Resolution worse than 50 km is denoted with the white coloration. (A) 7.5 s period Rayleigh waves. (B) 15 s period Rayleigh waves. Black solid lines are known active faults. Blue triangles are locations of the USArray stations used in this study. The resolution was estimated with the method of Barmin et al. (2001). This method does not account for finite-frequency diffraction effects nor for off-great circle propagation and, therefore, provides rather optimistic estimates of the resolution. To obtain more realistic and conservative estimates the values shown here should be multiplied by about a factor of 2.